Evaluation of point-forcing models with application to vertical axis wind turbine farms

By B. Pierce, P. Moin AND J. Dabiri

1. Motivation and objectives

Vertical axis wind turbines (VAWTs) have recently emerged as an area of research as an alternative to horizontal axis wind turbines (HAWTs). On an individual turbine basis, VAWTs are less efficient and produce less power than HAWTs. However, Kinzel *et al.* (2012) have shown that there is a possibility for VAWTs to produce a higher power density (power per area) than that of HAWTs. The investigation of Kinzel *et al.* (2012) was limited to a small turbine array (eighteen turbines), and thus further investigation is needed to determine if higher power densities can be achieved. Toward this end, Craig *et al.* (2013) have begun experiments of arrays of circular cylinders in a water channel. This configuration will serve as a model problem for the turbine array to investigate farm-scale effects and determine how rotation rates and turbine placements effect power density.

Our goal is to explore the farm-scale effects (both for the model problem of a cylinder array as well as the original problem of a farm of VAWTs) using large eddy simulation. The Reynolds number of the VAWT farm ($\mathcal{O}(10,000,000)$) is such that using a mesh that resolves the turbine blade and the flow scales at the blade would have a prohibitive cost. Additionally, because the arrangement of the VAWTs within the farm will not necessarily be uniform and the rotation direction of the turbines can be varied as well (with some rotating clockwise and other counterclockwise in an irregular pattern), the entire farm of VAWTs must be included in the computation (as opposed to including a minimum number of turbines and using periodic boundary conditions as is often done in wind farm studies). These constraints (the high Reynolds number of the flow and the necessity to include many turbines in the calculation) do not exist for the model problem of flow through a rectangular array of cylinders in a water channel, but we require that any model we develop for flow through the array of cylinders should be easily extended to the VAWT farm.

Kinzel *et al.* (2012) showed that certain aspects of a vertical axis wind turbine farm resembles a canopy flow. Recently, Dupont *et al.* (2010) used a drag forcing model to study canopy flows. The essential component of the model is to treat the interaction of the flow with the obstacle (in their case a crop) using a point force (which is always spread over multiple grid points for numerical reasons). Although this approach has some similar features to the well-known immersed-boundary method, it provides less fidelity because the shape of the object is not included. The approach of Dupont *et al.* (2010) (and many other canopy flow simulations, including Schlegel *et al.* 2012 and Yue *et al.* 2008) has an analog in HAWT calculations called the actuator approach. Various degrees of fidelity exist for actuator approaches, including actuator disk, actuator line, and actuator surface. The introduction in Sanderse (2013) contains an excellent review on work in actuator methods. Although actuator line and surface methods differ from the

point-forcing methods of canopy flows in wind turbine applications, both point-forcing and actuator methods reduce to the same form for a solid cylinder.

In this paper, we employ the point-forcing method (or equivalently, the reduction of the actuator line method for a circular cylinder) to simulate the model problem of flow through an array of cylinders. In Section 2 we present the formulation of the model as well as some details on the discretization of the forcing term. In Section 3 we demonstrate the performance of the model for flow over a single cylinder and flow through an array of cylinders (both cases include stationary and rotating cylinders). Finally in Section 4 we provide some concluding remarks.

2. Formulation

The point-forcing model is implemented within the framework of large eddy simulation. The governing equations which are solved are

$$\frac{\partial \overline{u}_i}{\partial t} + \frac{\partial \left(\overline{u}_i \overline{u}_j\right)}{\partial x_j} = -\frac{\partial \overline{p}}{\partial x_i} + \left(\nu + \nu_{\mathrm{SGS}}\right) \frac{\partial^2 \overline{u}_i}{\partial x_j \partial x_j} + f_i, \tag{2.1}$$

where the density is taken as unity and ν_{SGS} is computed using the dynamic Smagorinsky model from Germano *et al.* (1991) with the modification of Lily (1992). The forcing term $f_i = f_{i,D} + f_{i,L}$ is taken in a similar form to Dupont *et al.* (2010) and is given by

$$\mathbf{f}_D = -\frac{C_D(\hat{\Omega})}{D} \left(\mathbf{u}_{\mathrm{cyl}} \cdot \mathbf{u}_{\mathrm{cyl}}\right)^{1/2} \mathbf{u}_{\mathrm{cyl}}, \tag{2.2a}$$

$$\mathbf{f}_L = -\frac{C_L(\hat{\Omega})}{D} \left(\mathbf{u}_{\mathrm{cyl}} \cdot \mathbf{u}_{\mathrm{cyl}}\right)^{1/2} \mathbf{u}_{\mathrm{cyl}} \times \mathbf{k}, \tag{2.2b}$$

where $\hat{\Omega} = D\Omega/U_\infty$ is the non-dimensional rotation rate of the cylinders (Ω is the dimensional rotation rate), and C_D and C_L are the experimental drag and lift coefficients, modified by an induction factor (see Calaf *et al.* 2010), and D is the diameter of the cylinder. To improve the numerical stability of the forcing term, it is spread out over a small region in the vicinity of the cylinder in a Gaussian manner (similar to Calaf *et al.* 2010). The width of the Gaussian used is a tunable parameter of the model but should be chosen to be reasonably close to the cylinder diameter. In our work, we tune the parameter such that it gives the best comparison with the experiment for flow over a single cylinder and then use the same value for flow through the array of cylinders. The cylinder velocity $\mathbf{u}_{\mathrm{cyl}}$ of equation (2.2) is computed using the same Gaussian as in the spreading of the cylinder forcing. The location for computing the cylinder velocity $\mathbf{u}_{\mathrm{cyl}}$ was varied from the cylinder center to three diameters upstream of the cylinder center, and no significant impact on the results was found if the induction factor was changed appropriately. Thus the location where $\mathbf{u}_{\mathrm{cyl}}$ is computed is not considered one of the tunable parameters of the model.

Equation (2.1) is solved using the discretization from Ham & Iaccarino (2004) and Ham *et al.* (2006) using the solver *cliff* from Cascade Technologies, Inc. The implementation is implicit and has second order accuracy in space and time.

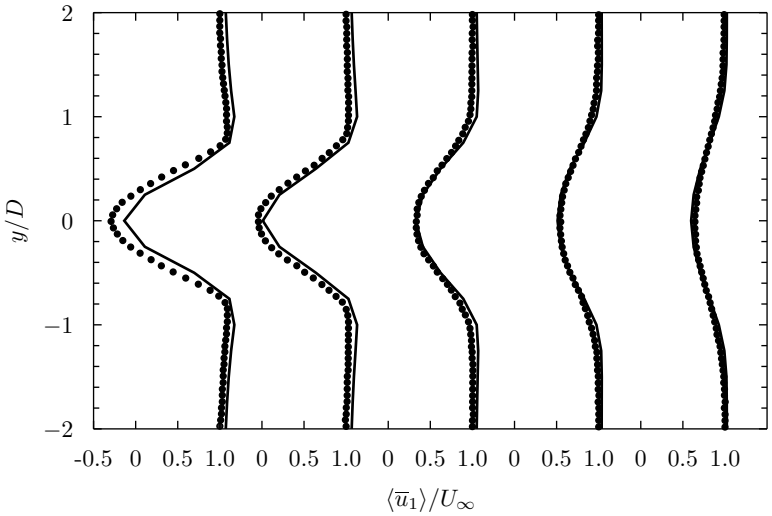

FIGURE 1. Mean streamwise velocity profiles, $\langle \overline{u}_1 \rangle$ as a function of vertical coordinate y/D at various locations $x/D = 1.2, 1.5, 2.0, 2.5, 3.0$ from left to right, with $x/D = 0$ corresponding to the cylinder center for a stationary cylinder. The lines are the results for the modeled computation, and the symbols are from the DNS of Mittal & Balachandar (1997).

3. Results

3.1. *Flow over a single cylinder at* $Re = 300$

For our initial model validation and testing, we compute the flow over a single cylinder at $Re = U_\infty D/\nu = 300$. We consider the cases of both a stationary and a rotating cylinder. For the stationary cylinder, we compare our results to the direct numerical simulation (DNS) of Mittal & Balachandar (1997). For the rotating cylinder, we have run our own DNS. The boundary condition upstream of the cylinder is a plug flow at U_∞, and the downstream boundary condition is a convective outflow. The spanwise boundary conditions are periodic, and the vertical boundary condition is a no-stress condition. The domain is chosen to be sufficiently large such that the boundaries are far away from the cylinder wake, and thus the boundary conditions do not effect the solution near the cylinder and in the region of interest for the wake behind the cylinder. The region of interest for the wake is confined to within $20D$, which is the same order as the cylinder spacing in the cylinder array configuration. The mesh for the modeled implementation has approximately $180,000$ grid points. The finest resolution, which is located around the center of the cylinder and in its near wake, is $\Delta x_{\min} = 0.25$. The modeled calculation uses a factor of ten fewer grid points in comparison to a DNS, which uses the same numerical scheme.

Figure 1 shows the evolution of the mean streamwise velocity in the wake of a single, stationary cylinder. The cylinder center is located at $x/D = 0$. Clearly the model is inaccurate immediately downstream of the cylinder (at around $x/D = 1.2$). However, as one travels downstream the comparison becomes much better so that by $x/D = 3.0$ the agreement is very good. Although not shown here, we have performed a grid convergence study and shown that this resolution is sufficiently fine such that this modeled solution is independent of the grid.

Figure 2 displays the evolution of the kinetic energy profiles in the wake of the cylinder (with the same data locations as Figure 1). Here we see that despite the relatively good

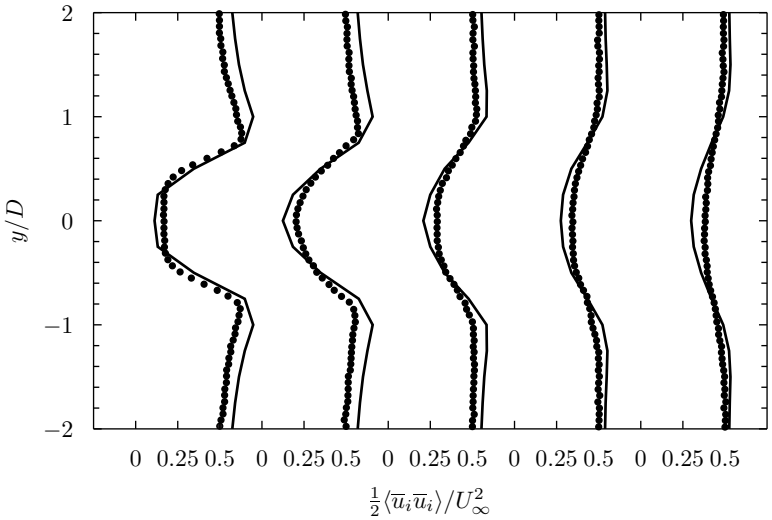

FIGURE 2. Mean kinetic energy profiles, $\langle\overline{u}_1\rangle$ as a function of vertical coordinate y/D at various locations $x/D = 1.2, 1.5, 2.0, 2.5, 3.0$, with $x/D = 0$ corresponding to the cylinder center for a stationary cylinder. The lines are the results for the modeled computation, and the symbols are from the DNS of Mittal & Balachandar (1997).

agreement of the mean velocity profile with the DNS at downstream locations ($x/D =$ 2.5, 3.0), the kinetic energy profiles have noticeable discrepancies. Figure 3 demonstrates that these discrepancies come from the vertical velocity fluctuations ($\langle\overline{u}_2'\overline{u}_2'\rangle$), which are under-predicted in the wake center. The streamwise velocity fluctuations are predicted quite well, although not shown here. This discrepancy in the vertical velocity fluctuations is an example of the difficulty that the model has in generating velocity fluctuations in directions perpendicular to the flow. The same difficulty results in a lack of three dimensional rib-like vortical structures that are viewed in the DNS, and as is seen below, causes further difficulties when the wake is not symmetric. This deficiency does not result from a lack of unsteadiness in the model. Although the lift coefficient is zero for the stationary cylinder and thus the lift term is not included, the drag force is unsteady and has a component in the vertical direction (although that component is zero in the mean).

Figure 4 shows the development of the mean streamwise velocity for a rotating cylinder with $\hat{\Omega} = 1.5$. The drag and lift coefficients for this case are taken from Mittal & Kumar (2003) and are $C_D = 0.8$ and $C_L = 4.0$. Here we see discrepancies that can be viewed as a combination of two errors. The first error is in the value of the minimum velocity, which was also seen in the stationary case. The second error regards the location of the wake in space, which can be identified by the location of the minimum $\langle\overline{u}\rangle$. To demonstrate the discrepancy in wake location more clearly, Figure 5 shows the wake location as a function of x/D for both the DNS and the model. Evidently, the point-forcing model is unable to capture the effect that increasingly pushes the wake away from the center. This is the same deficiency of the vertical fluctuating velocities seen in the stationary cylinder case, although here the inability to produce the correct vertical fluctuations also causes the location of the wake to be incorrect. Although the results shown here are only for the case of $\hat{\Omega} = 1.5$, we have examined other values of $\hat{\Omega}$ for the model and seen the same deficiencies.

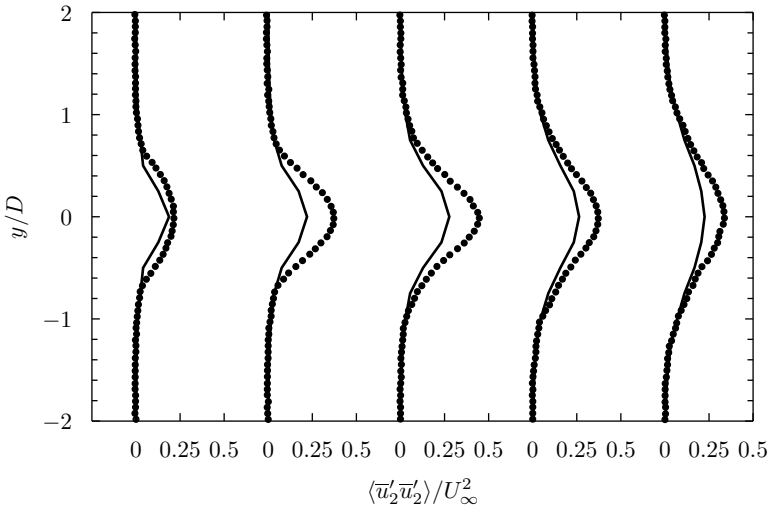

FIGURE 3. Mean vertical velocity fluctuation profiles, $\langle \overline{u}_1 \rangle$ as a function of vertical coordinate y/D at various locations $x/D = 1.2, 1.5, 2.0, 2.5, 3.0$, with $x/D = 0$ corresponding to the cylinder center for a stationary cylinder. The lines are the results for the modeled computation, and the symbols are from the DNS of Mittal & Balachandar (1997).

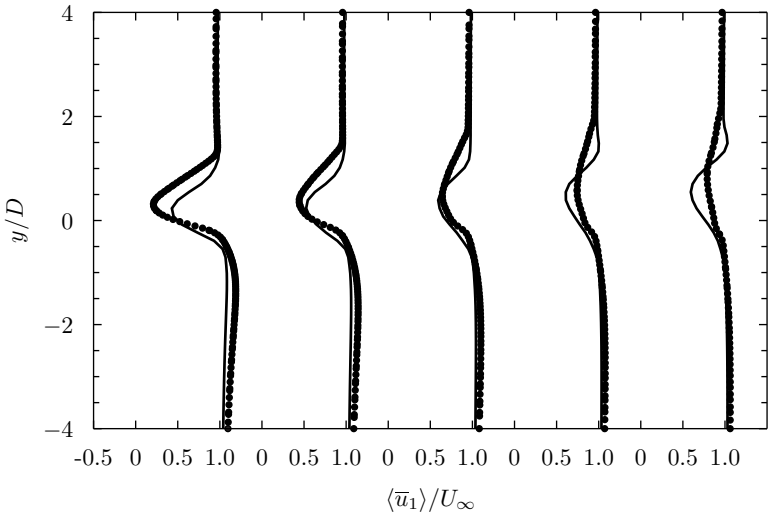

FIGURE 4. Mean streamwise velocity profiles, $\langle \overline{u}_1 \rangle$ as a function of vertical coordinate y/D at various locations $x/D = 1.2, 1.5, 2.0, 2.5, 3.0$, with $x/D = 0$ corresponding to the cylinder center for a cylinder with $\hat{\Omega} = 1.5$. The lines are the results for the modeled computation, and the symbols are from our DNS.

3.2. *Flow through a model VAWT farm*

Here we compute the flow through an array of cylinders that is serving as a model VAWT farm. The flow configuration is set to model the experiment performed by Craig *et al.* (2013). The experiment involves the flow of water in an open channel with a ten-by-ten array of circular cylinders in the center of the channel. Because the aspect ratio of the channel is relatively small, the side walls are included in the calculation. The channel

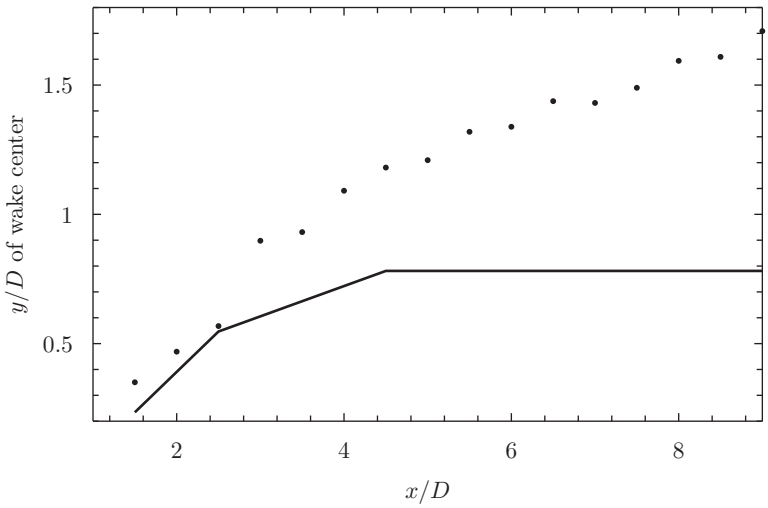

FIGURE 5. Vertical location y/D of the center of the wake behind a cylinder rotating with $\hat{\Omega} = 1.5$, as a function of streamwise coordinate x/D. The lines are the results for the modeled computation, and the symbols are from our DNS.

Reynolds numbers of the flow is $Re = U_\infty H_D/\nu = 96,000$, where U_∞ is the free stream velocity in the channel and H_D is the hydraulic diameter of the channel. Experimental measurements taken upstream of the cylinder array were used to estimate the friction Reynolds number of the boundary layer of the open channel as $Re_\tau = u_\tau \delta/\nu = 440$. Note that the experimental open channel is not long enough so that it can be considered a fully developed open channel. However, the experiment measured velocity profiles upstream of the cylinder array so that the most critical components of the inflow to the cylinder array could be matched. For these calculations, we resolve the flow at the wall. Future experimental configurations will most likely require the use of wall modeling to keep the calculation cost practical, as the Reynolds numbers of an actual VAWT farm are significantly higher.

For engineering purposes, the primary quantity of interest is the recovery of kinetic energy behind the cylinders. This will be the determining factor in the energy production for each turbine in a wind farm, and it is the primary quantity we consider here in evaluating the forcing model. The red line in Figure 6 shows the data location for Figures 7 and 9 (the data is taken in the direction of the flow). The data is located at the vertical coordinate $z/H_{\text{cyl}} = 0.43$, which is outside the boundary layer.

Figure 7 shows the kinetic energy recovery for the stationary cylinder case. The experimental values are shown with the symbols, and the agreement is reasonable. Note that the model parameters (including induction factor and spreading factor) were tuned for the case of the single cylinder at $Re = 300$. This is the behavior one would like to have in a model: it can be tuned in a case where one can expect to run an experiment (single cylinder or turbine), and it gives good results for the quantity of interest in the farm configuration. Figure 8 shows spanwise velocity profiles (see caption for data location within array). Although there are some minor discrepancies (which could in fact be cause by experimental noise), the overall agreement is good. Clearly, this model performs well for the case of stationary cylinders.

Figure 9 shows the kinetic energy recovery for the rotating cylinder case. Clearly the

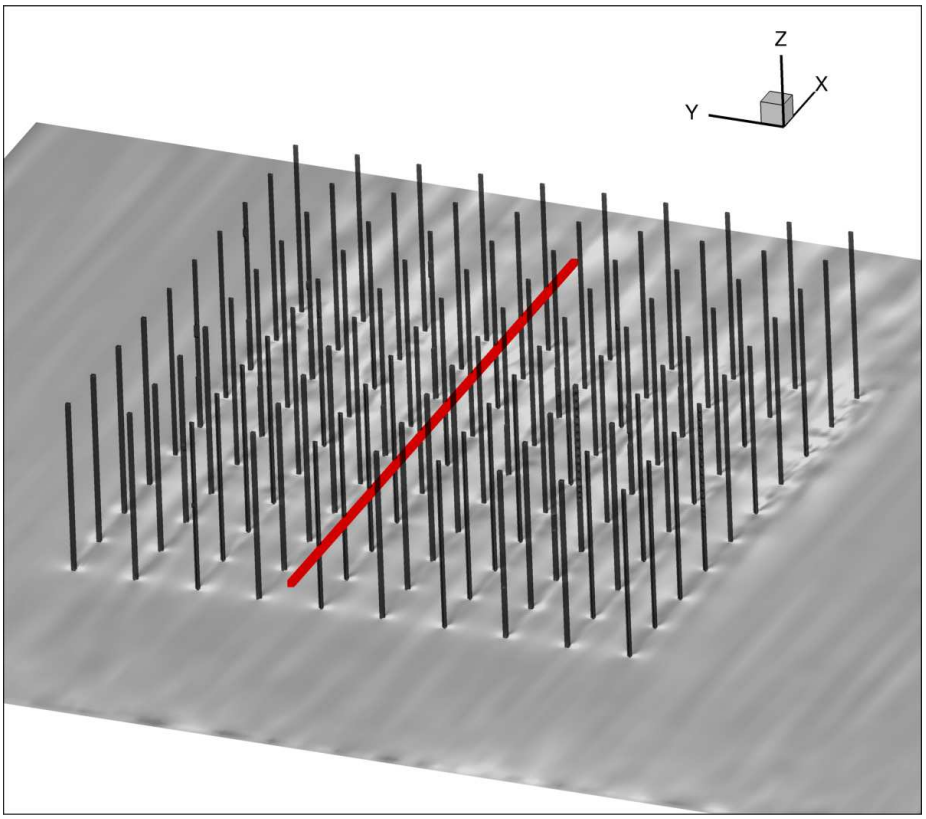

FIGURE 6. Location of data for Figure 7 and 9 (indicated by red line). The data begins ten cylinder diameters upstream of the array $x/D = -10$ and extends ten cylinder diameters behind the array ($x/D = 91$). The vertical coordinate is kept at $z/H_{\text{cyl}} = 0.43$. The spanwise location is immediately behind one of the two center-most cylinders in the array. The line is the result from the modeled computation and the symbols are from the experiment of Craig *et al.* (2013).

comparison with the experiment is poor. We have included the experimental results for the stationary case on this plot as well, which makes it clear that in the experiment, adding rotation of the cylinders causes the kinetic energy recovery to be greatly improved. It is evident that the model misses this impact entirely. The most likely cause of this gross under prediction is that the wakes are not pushed sufficiently far away from the cylinders in the spanwise direction and thus the wakes do not interact between the counter-rotating cylinders, thereby resulting in decreased mixing and kinetic energy recovery. In order to rule out model parameter choice as a cause of the under prediction, a wide range of parameters were tested. However, the choice was not found to improve the kinetic energy recovery, indicating that the deficiency in the model is not related to the choice of parameters but to the form of the forcing itself.

4. Conclusion

We have demonstrated the performance of the point-forcing model for flow over a single cylinder and flow through an array of cylinders. The model parameters were tuned for the single cylinder case and then applied to the array of cylinders. For the case of stationary

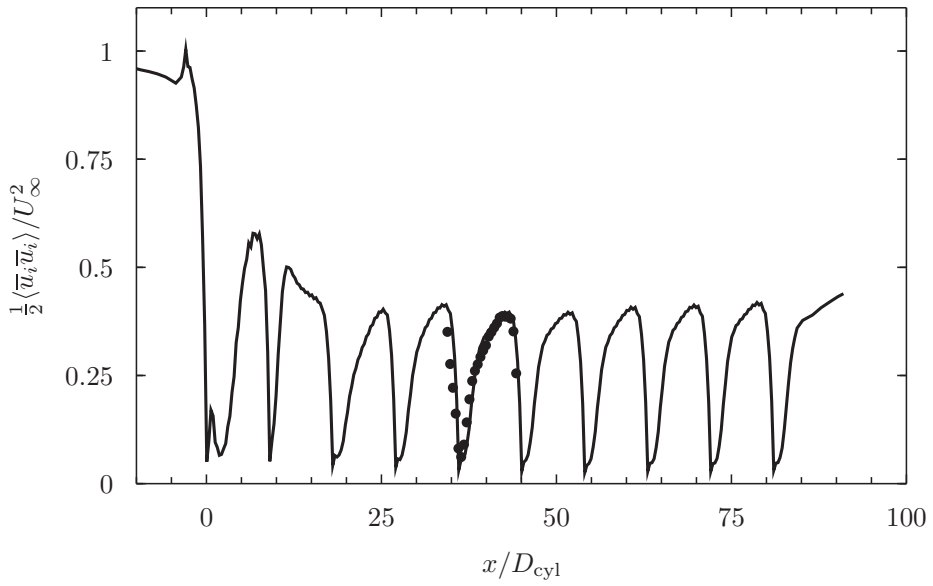

FIGURE 7. Mean kinetic energy behind an array of stationary cylinders (see Figure 6 for precise location of this data) as a function of streamwise coordinate x/D. The simulation data is the blue line and the experimental data is the black points. The line is the result from the modeled computation and the symbols are from the experiment of Craig *et al.* (2013).

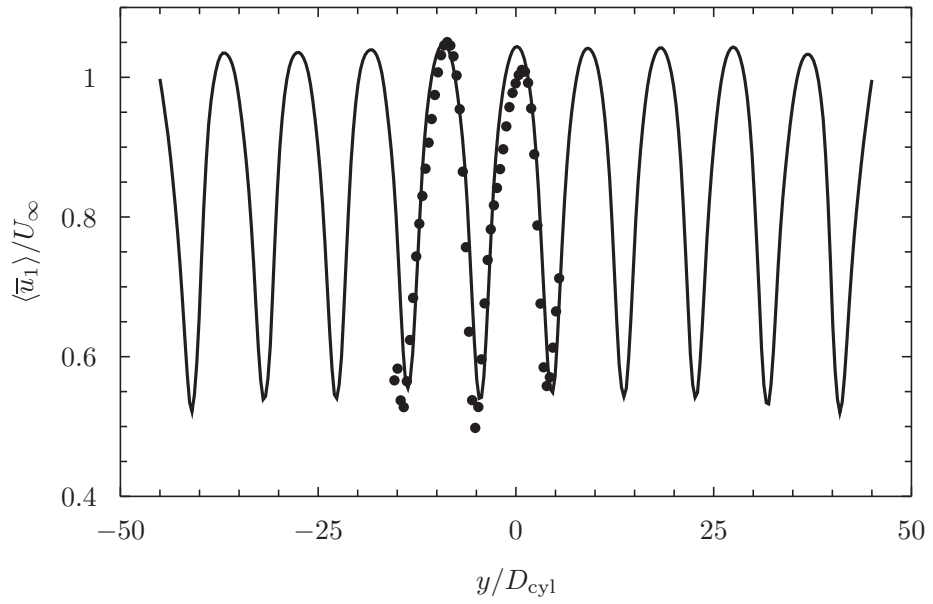

FIGURE 8. Mean velocity profiles as a function of the spanwise coordinate y/D for an array of stationary cylinders, taken at a height $z/H = 0.43$ and taken at the same height, $z/H = 0.43$, and taken between the fifth and sixth cylinder in the array. The line is the result from the modeled computation and the symbols are from the experiment of Craig *et al.* (2013).

cylinder(s), the model performed quite well. In particular, the recovery of the mean kinetic energy (which is the quantity of interest for a VAWT farm) was predicted extremely well.

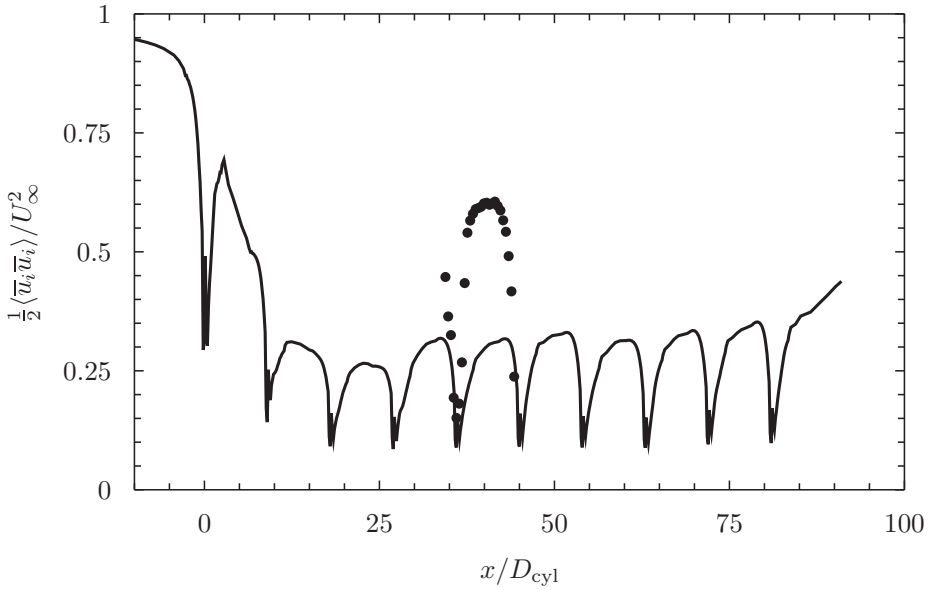

FIGURE 9. Mean kinetic energy behind an array of rotating cylinders ($\hat{\Omega} = 1.67$). See Figure 6 for a more detailed description of data location within the array. The line is the result from the modeled computation and the symbols are from the experiment of Craig *et al.* (2013).

Additionally, the mean velocity profiles in the spanwise direction compared well with experimental data.

However, for the case of rotating cylinders the prediction was very poor. The interaction of the wakes in the case of an array of counter-rotating cylinders is the cause of the higher kinetic energy recovery for rotating cylinders observed in the experimental data. The poor performance of the model in the simulation of the array of rotating cylinders can be attributed to the inability of the model to push the wake of the cylinder to the appropriate location. In fact, no set of model parameters was able to provide a good comparison between the simulation and experimental data. The fact that adjusting the model parameters in an ad hoc manner did not improve the kinetic energy recovery suggests that the point forcing model is incapable of modeling the effects of rotating cylinders. Thus, the future work will include exploring additional models, which include immersed boundary methods as well as other variants of the actuator type models.

Acknowledgments

The authors acknowledge computing and visualization time on the Certainty cluster at Stanford (MRI-R2 NSF Award 0960306). Additionally, Brian Pierce acknowledges the support from the Stanford Graduate Fellowship.

REFERENCES

Calaf, M., Meneveau, C. & Meyers, J. 2010 Large eddy simulation of fully developed wind-turbine array boundary layers. *Phys. Fluids* **22** (1), 015110.

Craig, A., Zellar, R., Zarama, F., Weitzman, J., Dabiri, J. & Koseff, J. 2013 The horizontal planar structure of kinetic energy in a model vertical-axis wind turbine array. APS DFD Conf.

Dupont, S., Gosselin., F., Py, C., Langre, E. D., Hermon, P. & Brunet, Y. 2010 Modelling waving crops using large-eddy simulation: comparison with experiments and a linear stability analysis. *J. Fluid Mech.* **652**, 5–44.

Germano, M., Piomelli, U., Moin, P. & Cabot, W. H. 1991 A dynamic subgrid-scale eddy viscosity model. *Phys. Fluids* **3** (7), 1760–1765.

Ham, F. & Iaccarino, G. 2004 Energy conservation in collocated discretization schemes on unstructured meshes. In *Annual Research Briefs*, pp. 3–14. Center for Turbulence Research.

Ham, F., Mattsson, K. & Iaccarino, G. 2006 Accurate and stable finite volume operators for unstructured flow solvers. In *Annual Research Briefs*, pp. 243–261. Center for Turbulence Research.

Kinzel, M., Mulligan, Q., & Dabiri, J. O. 2012 Energy exchange in an array of vertical-axis wind turbines. *J. Turb.* **13** (1).

Lily, D. K. 1992 A proposed modification of the Germano subgrid-scale closure method. *Phys. Fluids* **4** (3), 633–635.

Mittal, S. & Balachandar, R. 1997 On the inclusion of three-dimensional effects in simulations of two-dimensional bluff body wake flows. *ASME Fluids Eng. Divison Summer Meeting* .

Mittal, S. & Kumar, B. 2003 Flow past a rotating cylinder. *J. Fluid Mech.* **476** (4), 303–334.

Sanderse, B. 2013 Energy-conserving discretization methods for the incompressible Navier-Stokes equations. PhD thesis, Eindhoven University of Technology.

Schlegel, F., Stiller, J., Bienert, A., Maas, H.-G., Queck, R. & Bernhofer, C. 2012 Large-eddy simulation of inhomogeneous canopy flows using high resolution terrestrial laser scanning data. *Boundary-layer Meteorology* **142** (2), 223–243.

Yue, W., Meneveau, C., Parlange, M. B., Zhu, W., Kang, H. S. & Katz, J. 2008 Turbulent kinetic energy budgets in a model canopy: comparisons between LES and wind-tunnel experiments. *Environ. Fluid Mech.* **8** (1), 73–95.